

Catalytic graphitization of Electrospun Cellulose Nanofibres Using Silica Nanoparticles

Libo Deng^{a,b}, Anna E. Lewandowska^b, Robert J. Young^c, Guoping Zhang^a, Rong Sun^{a*}, Stephen J. Eichhorn^{b*}

^a Shenzhen Institutes of Advanced Technology, Chinese Academy of Sciences, Shenzhen, 518055, China

^b Physics/Engineering, College of Engineering, Mathematics and Physical Sciences, Physics Building, Stocker Road, University of Exeter, Exeter, EX4 4QL, UK.

^c Materials Science Centre, School of Materials, Grosvenor Street, University of Manchester, Manchester, M13 9PL, UK

Abstract

Electrospun cellulose nanofibres have been graphitized in the presence of silica (SiO₂) nanoparticles. The structure of the resultant SiC/C hybrids was characterized using transmission electron microscopy, X-ray diffraction and Raman spectroscopy. Bamboo-like silicon carbide (SiC) nanostructures were observed emanating from the nanofibres treated at 1500 °C which were thought to grow through a vapor-liquid-solid process. The formation of SiC was also thought to lead to a higher degree of graphitization for the electrospun cellulose fibres. These porous and graphitized nanofibres might find applications in electrochemical energy storage.

1. Introduction

There has been considerable interest in the use of graphitic nanostructures such as nanotubes and graphene as catalysts for the production of carbon fibres [1, 2]. Silica is a new and rapidly developing graphitization catalyst which has been investigated extensively [3-5]. Huang *et al.* have prepared single-walled carbon nanotubes through a chemical vapour deposition process using silica nanoparticles as the catalyst [6]. Medina *et al.* have demonstrated the direct growth of nanographene on silica at a low

* Corresponding Authors. Tel: +44 (0) 1392 72 5515; Fax: +44 (0) 1392 217965; email: s.j.eichhorn@exeter.ac.uk; rong.sun@siat.ac.cn

temperature (400 °C) [7]. There is no agreement however on whether SiO₂ transforms to SiC or it remains stable, and if any liquid forms during the reaction when SiO₂ is used as a graphitization catalyst. It has been suggested that the oxides of silicon are catalytically active for the graphitization of carbon, and that no SiC is involved in the graphitization process [8, 9]. On the other hand, it has also been demonstrated that nano-sized SiO₂ transforms to SiC, which then serves as the catalyst for the growth of graphitic nanostructures at a temperature as low as 400 °C [7].

Our previous studies have shown that electrospun cellulose nanofibres are an excellent precursor for the production of carbon fibres which might find potential applications as reinforcements in composite materials [10] and as electrode materials for supercapacitors [11]. Nanofibres however treated at 1500 °C exhibited only a low degree of graphitization with a low level of structural order. In the present study, SiO₂ nanoparticles were used to promote graphitization during pyrolysis of electrospun cellulose fibres. The structures of the resulting fibres were characterized using transmission electron microscopy (TEM), X-ray diffraction (XRD) and Raman spectroscopy. Bamboo-like SiC nanostructures were observed growing from the carbonized nanofibres, accompanied by a higher degree of stacking order and in-plane order for the carbon crystallites. The C/SiC hybrids also had a larger specific surface area than the pristine carbon nanofibres and therefore might possess a higher electrochemical capacitance when used as electrode materials for supercapacitors.

2. Experimental

2.1 Materials

Cellulose acetate (CA, average $M_n = 100,000 \text{ g mol}^{-1}$), SiO₂ nanoparticles (with diameters in the range of 10- 20 nm), acetone, N, N-dimethylacetamide (DMAc), were purchased from Sigma-Aldrich.

2.2 Preparation of the cellulose nanofibres

Cellulose acetate (CA) was dissolved in a mixed solution of acetone and N,N-dimethylacetamide and was electrospun into CA nanofibres. The CA nanofibres were then deacetylated in a NaOH/ethanol, which yielded cellulose nanofibres. The details of this process have been described in our previous work [10].

2.3 Carbonization of the electrospun fibres

Graphitization of the fibres was carried out using a Carbolite CTF16/75 furnace. Mats of cellulose nanofibres were placed in a graphite boat, sitting on top of SiO₂ nanoparticles. Typically 50 mg of the nanofibre mats was placed on top of 10 mg of SiO₂ nanoparticles. The nanofibres were then stabilized initially by heating to 240 °C in air at a rate of 3 °C/min, followed by a 60 minute isotherm at the final maximum temperature. The stabilized fibres were then carbonized by heating at a rate of 10 °C/min, followed by a 150 minute isotherm at 1500 °C in an argon atmosphere.

2.4 Characterization of fibres

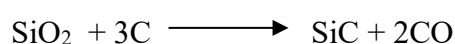
Raman spectra were obtained using a Renishaw system 1000 spectrometer coupled to an Argon-ion laser with a wavelength of 514 nm. The laser spot size was ~1-2 μm, and the power was ~1 mW when the laser is focused on the sample using an Olympus BH-1 microscope. Additionally, the measurements were performed with a Renishaw RM-1000 System. A 532 nm wavelength diode laser was focused on the samples using a ×50 objective lens.

The crystal structure of the fibres was examined using a Philips X'PERT APD powder X-ray diffractometer ($\lambda = 1.54 \text{ \AA}$, CuK α radiation). The samples were rotated within the X-ray diffractometer chamber to mitigate problems of preferred orientation. The morphology of the nanofibres was investigated after gold coating using a Philips XL30 FEG SEM, operated at an accelerating voltage of 5 kV. Carbon nanofibre (CNF) bundles were sonicated in ethanol for 10 min, deposited onto TEM grids and examined using a Philips CM20 TEM to investigate their microstructures. The surface area of the carbon nanofibres was measured using the Brunauer-Emmett-Teller (BET) nitrogen adsorption method with a Coulter SA3100 instrument. The fibres were degassed under vacuum at 120 °C for 4h before the BET measurements.

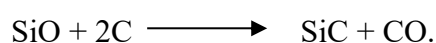
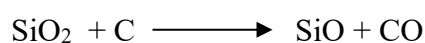
3. Results and discussion

Figure 1a and 1b show SEM images of the cellulose electrospun fibres and the fibres produced by treating cellulose/SiO₂ at 1500 °C. It can be seen upon heat treatment, the fibrous structure of the precursor was retained. The average diameter of the nanofibres derived from the cellulose/SiO₂ mixture was ~200 nm which is close to that of the

pristine carbon nanofibres. TEM observations revealed bamboo-like nanostructures in the carbon matrix (Figure 1c). Closer inspection (see Figure 1d, which was taken from the core region of the resultant composite fibre) indicated that these stacking layers consist of crystallites with a lattice spacing of ~ 0.26 nm which is typical of the 111 plane of SiC crystallites. It also suggests that the core also contains carbon phase. SiC in the fibre was thought to be formed through the carbothermal reduction of silica according to the overall reaction [3]



which can be broken down into two elementary steps:



SiC nanostructures have been observed in other carbothermal processes where a vapour-solid (VS) [12] or vapour-liquid-solid (VLS) [13] mechanism is usually involved. The melting point of SiO₂ nanoparticles used in this study is in excess of 1600 °C. It is inferred that the SiO₂ nanoparticles firstly soften at 1500 °C and react with the carbon which gives rise to the formation of SiO. The SiO then evaporates and diffuses into the core region of the CNF and reacts further with the carbon which yields SiC nanostructures. The growth of bamboo-like structures is thought to be similar to bubble-chain-like boron nitride nanotubes [14]. Their formation was explained by a pressure induced mutation mechanism. When the concentration of Si and C species are supersaturated in the SiO₂ melt, SiC nuclei begin to precipitate on the surface of the liquid drop and form a SiC cap. With the continuous supply of Si and C atoms, the cap grows gradually up into a bamboo-like SiC nanostructure.

Turbostratic carbon was observed from the edge of the fibre treated in the presence of SiO₂ at 1500 °C (Figure 1e). TEM observation shows that the stacking order and in-plane order for the carbon crystallites in the composite fibre was higher than in the pure CNF (Figure 1f). Furthermore, no SiC or obvious carbon crystallites were seen from the precursors treated even in the presence of SiO₂ at lower temperatures, suggesting that SiC is the catalytic active species in this case. A cable-like structure with SiC

nanowires as the core and carbon crystallites as the shell was observed by Ye *et al.* from pyrolysis of PAN nanofibres in a SiO atmosphere [15]. They explained that carbon crystallites formed through the deposition of carbon on SiC nanowires [15]. Kim *et al.* also prepared SiC-C coaxial nanocables that possessed graphitic shells. This was carried out by direct growth of SiC nanowires on silicon substrates and subsequent carbon deposition using pyrolysis of methane [16]. In all these cases, SiC instead of SiO₂ was thought to be the graphitization catalyst.

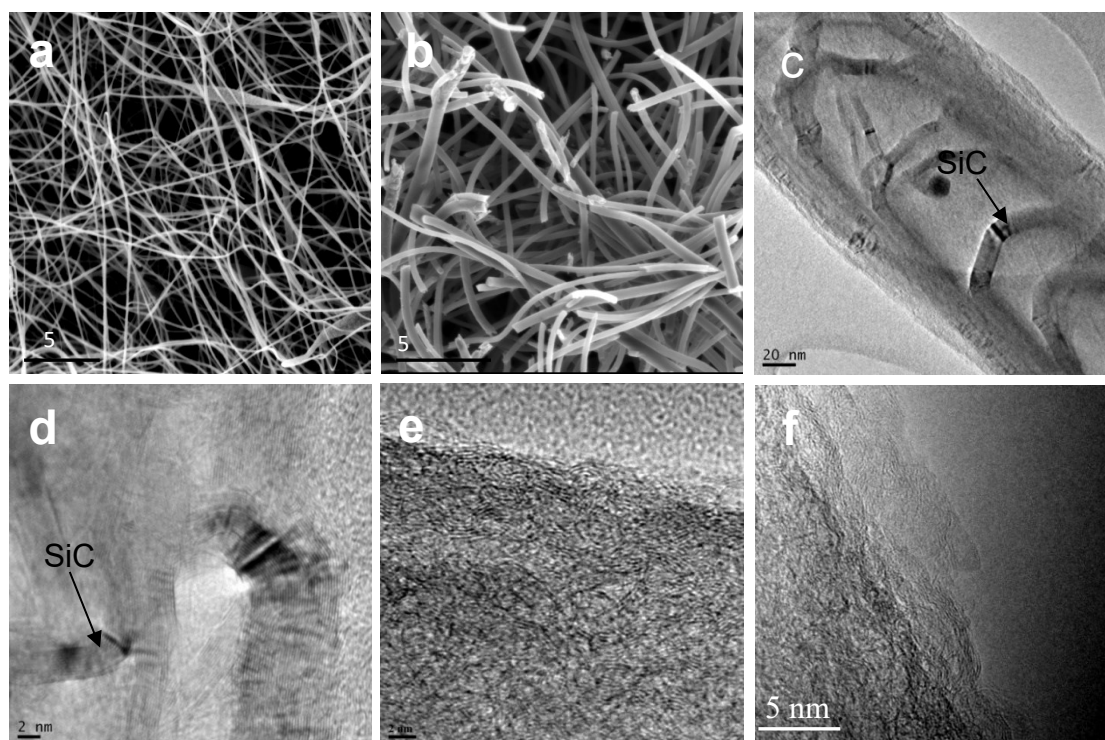


Fig. 1. (a) SEM image of the electrospun cellulose fibres; (b) SEM image of the C/SiC composite fibres; (c-e) TEM images of the C/SiC composite fibres; (f) TEM image of the pure CNF.

Figure 2 shows the XRD patterns for the CNFs derived from cellulose alone and cellulose/SiO₂. The broad peak at $\sim 25^\circ$ seen in the pure CNFs corresponds to the (002) crystallographic plane of a carbon crystallite, with a low crystallinity. This peak becomes significantly narrower in the C/SiC composite fibres, suggesting a larger L_c (the thickness along the 002 plane) and a higher stacking order in the latter. Additionally, seven peaks are distinguished in the XRD pattern corresponding to different polytypes of silicon carbide structures. The presence of three strong peaks at $2\theta = 35.7, 60.0$ and 71.8° can be assigned to 111, 220, and 311 lattice planes of β -SiC, respectively. The small peak at 33.7° is thought to be due to stacking faults which can be formed easily

during the growth of SiC nanostructures as crystal defects have lower energy than the perfect crystal planes [17]. The presence of the peaks with lower intensity near 38.0, 41.3 and 75.5° can be attributed to the SiC polytypes with a lower symmetry, such as 6H-SiC with a hexagonal lattice and 15R-SiC with a rhombohedral lattice. Both are classified as an α -SiC form. The lower symmetry structures also have peaks near 35.7, 60.0 and 71.8° overlapping with β -SiC form.

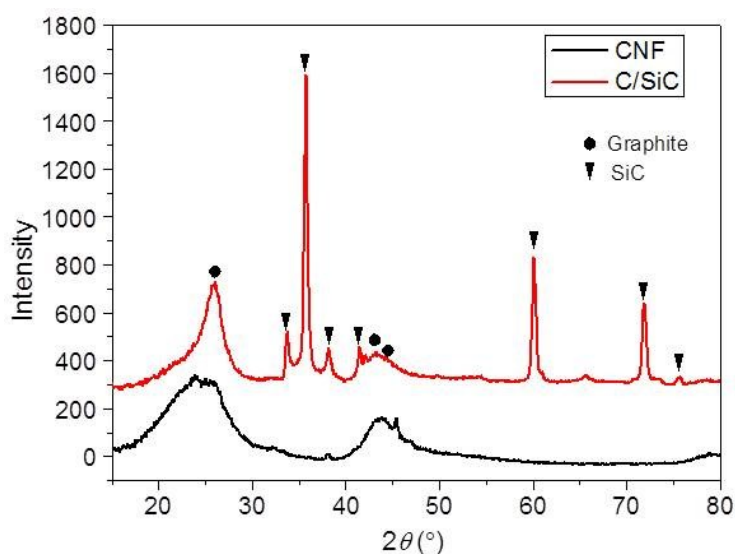


Fig. 2. XRD patterns of the CNFs derived from electrospun cellulose fibres alone and cellulose/SiO₂.

The composition of the resultant fibres was further characterised using Raman spectroscopy. Figure 4 shows a Raman spectrum of the C/SiC composite fibres. The spectrum for pure CNF carbonized at the same temperature is also shown for comparison. The most striking feature in the spectrum of the C/SiC composite is the narrow and strong 2D-band (located at $\sim 2715 \text{ cm}^{-1}$) which is almost as intense as the G-band (located at $\sim 1586 \text{ cm}^{-1}$). The profile of the 2D-band and the ratio of the intensities of the 2D and G band (I_{2D}/I_G) have been widely used to identify the number of graphene layers [18]. A value of ~ 1 for the I_{2D}/I_G and a full width at half maximum (FWHM) of 56 cm^{-1} for the 2D-band is usually seen for bi-layer graphene. It is unclear whether few-layer graphenes exist in our system but is safe to conclude that carbon crystallites with very high stacking order formed. The increase in graphitization relative to the pure CNF is further corroborated by other Raman features: The ratio of the intensities of the D-band to the G-band (I_D/I_G) is significantly lower and the FWHM for

all Raman bands are smaller than that for the pristine carbon nanofibres. The peaks at 768 cm^{-1} and $\sim 972\text{ cm}^{-1}$ correspond to the transverse optical (TO) and longitudinal optical (LO) modes of SiC [19], and the small FWHM of these peaks also suggest the formation of highly crystalline SiC. These findings are consistent with the XRD characterization.

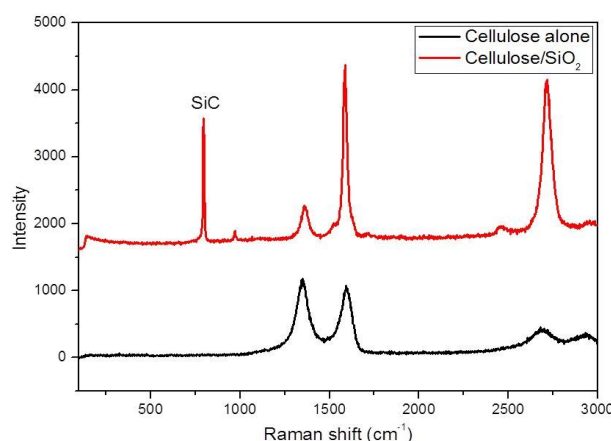


Fig. 3. Raman spectra of the CNFs derived from the electrospun cellulose fibres alone and cellulose/SiO₂.

Selected Raman spectra recorded at different points of C/SiC hybrids are reported in Figure 4. They show features characteristic for CNFs; sharp and well-defined first- and second order Raman bands. Raman band frequencies are shifted to the higher values (closer to the frequency of crystalline graphite). The D band is located at $\sim 1349\text{ cm}^{-1}$ ($\pm 3\text{ cm}^{-1}$), while the G band is centred at $\sim 1580\text{ cm}^{-1}$ ($\pm 2\text{ cm}^{-1}$). It is worth pointing out the presence of a well-defined 2D band centred at 2695 cm^{-1} ($\pm 4\text{ cm}^{-1}$). It suggests the presence of elevated structural order in the nanofibres and the development of graphitic structures in the material [20, 21]. It seems that a treatment of the electrospun cellulose fibres in the presence of SiO₂ particles facilitates the formation of graphite structure. On the other hands, it leads to a higher heterogeneity in the composition of the C/SiC hybrids obtained. The value of I_D/I_G ratio estimated to be 0.45 shows a high error value of ± 0.11 .

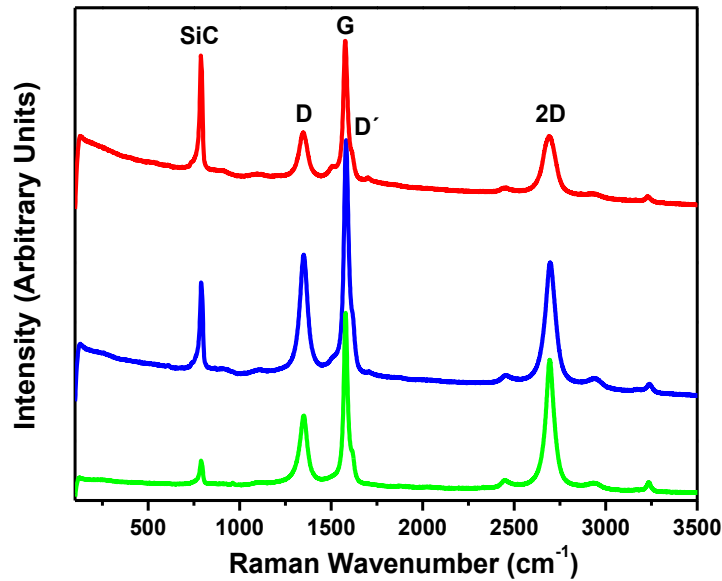


Fig. 4. Raman spectra recorded at different points of C/SiC hybrids.

Figure 5 shows splitting of the Raman band attributed to silicon carbide species. Raman bands centred at $\sim 970 \text{ cm}^{-1}$ correspond to the LO phonon mode, while bands located in the range $750 - 800 \text{ cm}^{-1}$ to the TO phonon mode [22, 23]. The TO phonon mode consists of Raman bands located at $\sim 770 \text{ cm}^{-1}$ ($\pm 2 \text{ cm}^{-1}$), $\sim 788 \text{ cm}^{-1}$ ($\pm 0.8 \text{ cm}^{-1}$) and $\sim 796 \text{ cm}^{-1}$ ($\pm 1 \text{ cm}^{-1}$) based on the fitting of the band with Lorentzian function. The band centred at $\sim 796 \text{ cm}^{-1}$ corresponds to the un-shifted $T_2(\text{TO})$ mode of bulk 3C-SiC with a cubic crystal structure (β -SiC), whereas the band at $\sim 788 \text{ cm}^{-1}$ caused by an effective reduction in symmetry is assigned to various polytypes, such as 6H-SiC ($E_{2(\text{high})}$ mode) with a hexagonal structure (α -SiC) and/or 15R-SiC ($2E$ mode) with a rhombohedral structure (α -SiC). The TO band is degenerate, therefore the reduction from cubic symmetry causes a shift of one of the TO component to lower wavenumber. The degeneracy is lost due to the formation of other polytypes or the introduction of random stacking faults [23]. Raman band at $\sim 770 \text{ cm}^{-1}$ may belong to 3C-SiC structure with a random distribution of stacking faults [24], but it is also close to the signal originating from the 6H-SiC ($E_{2(\text{low})}$ mode) [22]. A weak Raman band located at $\sim 962 \text{ cm}^{-1}$ corresponds to the $A_1(\text{LO})$ mode of hexagonal polytypes. The analysis of Raman bands confirms, that the silicon carbide consists of different polytypes [25].

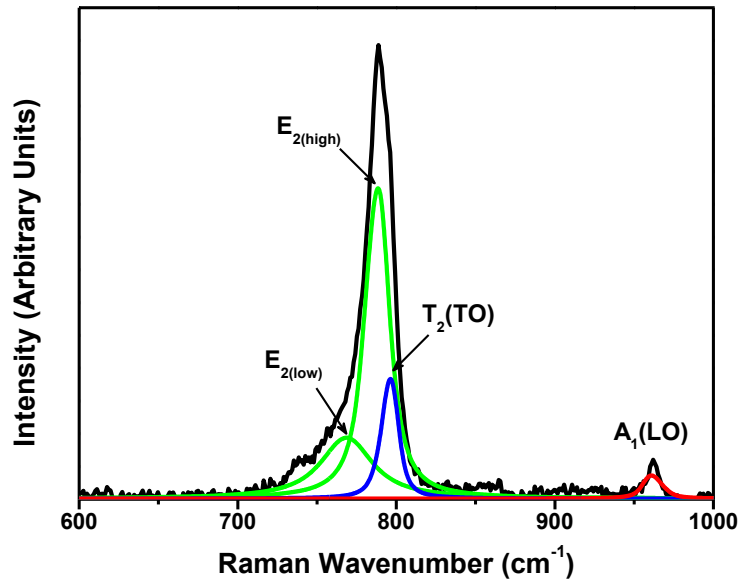


Fig. 5. Detail of the silicon carbide optical band region in Raman spectrum of C/SiC hybrids.

. Figure 6 shows the nitrogen adsorption curves for both the pristine carbon nanofibres and C/SiC hybrids. The steep adsorption at low relative pressure indicates a high level of microporosity. The specific surface area increased from $\sim 80 \text{ m}^2/\text{g}$ for the carbon nanofibres to $140 \text{ m}^2/\text{g}$ for the C/SiC hybrids. The porous structures of the fibres are thought to significantly increase their surface area. Our previous study showed that that activated carbon nanofibres have large electrochemical capacitance [11]. As the degree of graphitization (and possibly the electrical conductivity) and specific surface area of the C/SiC hybrids have been both increased compared to pristine CNF, the hybrids might also find application in supercapacitors. This remains a topic for future research.

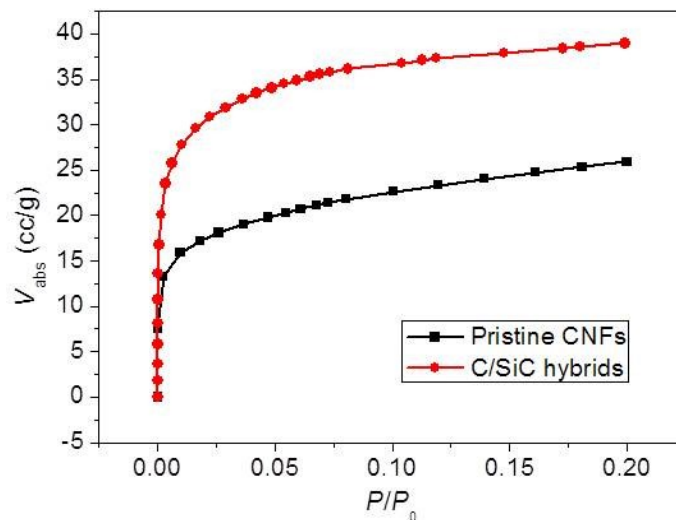


Fig. 6. Typical nitrogen adsorption curves for the pristine CNFs and C/SiC hybrids.

4. Conclusions

Carbonization of cellulose nanofibres at 1500 °C in the presence of SiO₂ nanoparticles has yielded bamboo-like SiC nanostructures in the carbon nanofibre matrix. This treatment also leads to a higher degree of graphitization than pristine carbon nanofibres. The SiC nanostructures were formed through a vapour-liquid-solid mechanism and were the catalytic active species for graphitization. The increase in graphitization and surface area might potentially lead to a higher electrochemical capacitance in supercapacitors.

Acknowledgements

This work was supported by EPSRC (EP/F036914/1 and EP/I023879/1), Universities of Exeter and Manchester, Guangdong and Shenzhen Innovative Research Team Program (No. 2011D052, KYPT20121228160843692), National Natural Science Foundation of China (Grant No. 21201175), R&D Funds for basic Research Program of Shenzhen (Grant No. JCYJ20120615140007998) and Shenzhen Electronic Packaging Materials Engineering Laboratory (Grant No. 2012372).

References

1. V. Jourdain, C. Bichara, *Carbon* 58 (2013) 2-39.
2. Z. Yan, Z. Peng, J. M. Tour, *Acc. Chem. Res.* 47 (2014) 1327-1337.
3. A. Bachmatiuk, F. Boerrnert, M. Grobosch, F. Schaeffel, U. Wolff, A. Scott, M. Zaka, J. H. Warner, R. Klingeler, M. Knupfer, *ACS Nano* 3 (2009) 4098-4104.
4. J. Chen, Y. Wen, Y. Guo, B. Wu, L. Huang, Y. Xue, D. Geng, D. Wang, G. Yu, Y. Liu, *J. Am. Chem. Soc.* 133 (2011) 17548–17551.
5. P. Y. Teng, C. C. Lu, K. Akiyama-Hasegawa, Y. C. Lin, C. H. Yeh, K. Suenaga, P. W. Chiu, *Nano Lett.* 12 (2012) 1379–1384.
6. S. Huang, Q. Cai, J. Chen, Y. Qian, L. Zhang, *J. Am. Chem. Soc.* 131 (2009) 2094–2095.
7. H. Medina, Y. C. Lin, C. H. Jin, C. C. Lu, C. H. Yeh, K. P. Huang, K. Suenaga, J. Robertson, P. W. Chiu, *Adv. Funct. Mater.* 22 (2012) 2123-2128.
8. M. H. Rummeli, C. Kramberger, A. Gruneis, P. Ayala, T. Gemming, B. Buchner, T. Pichler, *Chem. Mater.* 19 (2007) 4105-4107.
9. M. H. Rummeli, F. Schuffel, C. Kramberger, T. Gemming, A. Bachmatiuk, R. J. Kalenczuk, B. Rellinghaus, B. Buchner, T. Pichler, *J. Am. Chem. Soc.* 129 (2007) 15772-15773.

10. L. Deng, R. J. Young, I. A. Kinloch, Y. Zhu, S. J. Eichhorn, *Carbon* 55 (2013) 66-75.
11. L. Deng, R. J. Young, I. A. Kinloch, A. M. Abdelkader, S. M. Holmes, D. A. D. H.-D. Rio, S. J. Eichhorn, *ACS Appl. Mater. Interfaces* 5 (2013) 9983-9990.
12. R. Rajarao, R. Ferreira, S. H. F. Sadi, R. Khanna, V. Sahajwalla, *Mater. Lett.* 120 (2014) 65-68.
13. X. Qi, J. Liang, C. Yu, S. Ma, X. Liu, B. Xu, *Mater. Lett.* 116 (2014) 68-70.
14. J. L. Wang, L. P. Zhang, Y. L. Gu, X. Y. Pan, G. W. Zhao, Z. H. Zhang, *J. Exp. Nanosci.* 8 (2013) 833-841.
15. H. H. Ye, N. Titchenal, Y. Gogotsi, F. Ko, *Adv. Mater.* 17 (2005) 1531-1535
16. H. Y. Kim, S. Y. Bae, N. S. Kim, J. Park, *Chem. Commun.* (2003) 2634-2635.
17. G. Y. Li, X. D. Li, H. Wang, X. Xing, Y. Yang, *Mater. Sci. Eng., B* 166 (2010) 108-112.
18. A. C. Ferrari, J. C. Meyer, V. Scardaci, C. Casiraghi, M. Lazzeri, F. Mauri, S. Piscanec, D. Jiang, K. S. Novoselov, A. K. Geim, *Phys. Rev. Lett.* 97 (2006) 187401.
19. M. Bechelany, A. Brioude, D. Cornu, G. Ferro, P. Miele, *Adv. Funct. Mater.* 17 (2007) 939-943.
20. A. C. Ferrari, J. Robertson, *Phys. Rev. B* 61 (2000) 14095 1-13.
21. A. C. Ferrari, J. Robertson, *Phys. Rev. B* 64 (2001) 075414 1-13.
22. G. Chollon, *Thin Solid Films* 516 (2007) 388-396.
23. E. López-Honorato, C. Brigden, R. A. Shatwell, H. Zhang, I. Farnan, P. Xiao, P. Guillermier, J. Somers, *J. Nucl. Mater.* 433 (2013) 199-205.
24. S. Rohmfeld, M. Hundhausen, L. Ley, *Phys. Rev. B* 58 (1998) 9858-9862.
25. Y. Ward, R. J. Young, R. A. Shatwell, *J. Mater. Sci.* 39 (2004) 6781-6790.